

Chaos in Turbulence Driven by the Magnetorotational Instability

Wayne F. Winters, Steven A. Balbus, and John F. Hawley

Dept. of Astronomy, University of Virginia, PO Box 3818, Charlottesville, VA 22903, USA.

Accepted. Received.

ABSTRACT

Chaotic flow is studied in a series of numerical magnetohydrodynamical simulations that use the shearing box formalism. This mimics important features of local accretion disk dynamics. The magnetorotational instability gives rise to flow turbulence, and quantitative chaos parameters, such as the largest Lyapunov exponent, can be measured. Linear growth rates appear in these exponents even when the flow is fully turbulent. The extreme sensitivity to initial conditions associated with chaotic flows has practical implications, the most important of which is that hundreds of orbital times are needed to extract a meaningful average for the stress. If the evolution time in a disk is less than this, the classical α formalism will break down.

Key words: accretion disks — instabilities — MHD

1 INTRODUCTION

Astrophysical accretion disks are able to evolve because angular momentum is extracted from fluid elements and transported outward. This is effected by the presence of non-vanishing radial-azimuthal components of the Maxwell and Reynolds stress tensors, produced by magnetohydrodynamic (MHD) turbulence driven by the magnetorotational instability (MRI) (Balbus & Hawley 1998). As there is no analytic theory of MHD turbulence at hand (nor is there one in sight), large-scale numerical simulation has been the main avenue of progress toward understanding its properties.

Many numerical studies make use of the local “shearing box” approximation (Hawley, Gammie & Balbus 1995). The shearing box is an invaluable tool for studying local flow dynamics in detail, and for resolving turbulent flow with the largest possible dynamical range. MHD turbulence, like all true turbulence, should be chaotic, as quantified formally by a measured positive Lyapunov exponent. What is less clear, but of great astrophysical significance, is whether long term flow averages are even well-defined. To put the question most starkly, imagine macroscopically identical disks, with fluid perturbations that vary by a tiny amount. The fine scale description of their internal turbulence will surely differ, but will quantities such as the stress tensor components converge to the same values in the long term? This question goes directly to the heart of the standard α disk formalism (Shakura & Sunyaev 1973) which assumes that disk transport may be described by a spatially constant or slowly varying α parameter. (The quantity α is defined as the ratio of radial-azimuthal component of the stress tensor

$T_{R\phi}$ to the gas, or gas plus radiation, pressure.) How well supported is this assumption?

This paper begins to study these complex issues by examining the chaotic nature of the MHD turbulence. The presentation is organized as follows. In §2 we briefly review the shearing box. In §3 we present the results of experiments designed to reveal how the measured properties of turbulent flow are related to both computational and physical input parameters. In §4, we carry out a series of experiments that demonstrate qualitatively that the MHD turbulence is chaotic, and in §5 this is quantified by computing the Lyapunov exponents for a set of simulations. Our conclusions are summarized in §6.

2 SHEARING BOX SYSTEM

The shearing box system, described in Hawley, Gammie & Balbus (1995), is designed to represent a very local section of an accretion disk, viewed in corotating coordinates with angular frequency Ω . Starting with the full set of dynamical equations in cylindrical coordinates, the equations are locally expanded about a fiducial cylindrical radius R , with (dx, dy, dz) corresponding to cylindrical coordinates $(dR, Rd\phi, dz)$. The computational domain is then a Cartesian box, but with the rotational inertial forces (Coriolis and centrifugal) retained. The centrifugal force nearly balances gravity, leaving a remnant tidal force linear in x . All other forces are directly retained. For this system, the ideal MHD equations of motion become,

$$\frac{\partial \mathbf{v}}{\partial t} + (\mathbf{v} \cdot \nabla) \mathbf{v} = -\frac{1}{\rho} \nabla \left(P + \frac{B^2}{8\pi} \right) + \frac{(\mathbf{B} \cdot \nabla) \mathbf{B}}{4\pi\rho} - 2\Omega \times \mathbf{v} + 2q\Omega^2 x \hat{\mathbf{x}} - \Omega^2 z \hat{\mathbf{z}}. \quad (1)$$

The mass conservation equation

$$\frac{\partial \rho}{\partial t} + \nabla \cdot (\rho \mathbf{v}) = 0, \quad (2)$$

the adiabatic internal energy equation,

$$\frac{\partial \rho \epsilon}{\partial t} + \nabla \cdot (\rho \epsilon \mathbf{v}) + P \nabla \cdot \mathbf{v} = 0, \quad (3)$$

and the induction equation

$$\frac{\partial \mathbf{B}}{\partial t} = \nabla \times (\mathbf{v} \times \mathbf{B}), \quad (4)$$

retain their usual forms. The internal energy per particle ϵ is defined by

$$P = \rho \epsilon (\gamma - 1). \quad (5)$$

For an isothermal gas, the energy equation is replaced with

$$P \rho^{-1} = \text{constant}. \quad (6)$$

The variables in these equations have their usual meanings. We shall also introduce the constant q , which is a parameter describing the local radial dependence of the angular frequency, i.e., $q = -d \ln \Omega / d \ln R$. For a Keplerian angular momentum distribution, $q = 3/2$. In this study we have ignored vertical gravity, and have thus dropped the $\Omega^2 z \hat{\mathbf{z}}$ term from equation (1).

These equations are solved using the time-explicit, operator-split finite differencing algorithm of the ZEUS code for hydrodynamics (Stone & Norman 1992a) and MHD (Stone & Norman 1992b; Hawley & Stone 1995). The shearing box computational domain extends in x , y , and z respectively from $-L_x/2$ to $+L_x/2$, 0 to L_y , 0 to L_z . The boundary conditions are periodic in both the y and z directions, and “shearing periodic” in x , meaning we equate

$$f(x, y, z) = f(x + L_x, y - q\Omega L_x t, z). \quad (7)$$

The azimuthal velocity has an additional correction to offset the angular velocity difference between the inner and outer radial boundaries:

$$v_y(x, y, z) = v_y(x + L_x, y - q\Omega L_x t, z) + q\Omega L_x. \quad (8)$$

The initial state is one of uniform density and pressure, and the velocity profile is $\mathbf{v} = -q\Omega x \hat{\mathbf{y}}$. In this paper, our initial magnetic field configurations are either a uniform toroidal magnetic field, or a vertical magnetic field varying sinusoidally in the radial x direction. The magnetic field strength is described by the standard plasma β parameter

$$\beta \equiv \frac{8\pi P}{B^2}, \quad (9)$$

the ratio of the gas to magnetic pressures. The MRI is triggered by seeding the initial equilibrium state with small pressure and velocity fluctuations.

3 SATURATION AMPLITUDE IN THE SHEARING BOX: A SURVEY

One of the goals of shearing box simulations has been to try to understand what determines the sustained saturation amplitude of the MRI-driven turbulence. In accretion disk applications, the focus is often on the $T_{r\phi}$ component of the combined Reynolds and Maxwell stress tensor,

$$T_{r\phi} = (-B_x B_y / 4\pi + \rho v_x \delta v_y). \quad (10)$$

Here δv_y is the azimuthal velocity fluctuation, obtained by subtracting the equilibrium shear flow. This can be directly measured in shearing box simulations. The volume-averaged stress is usually normalized to the averaged gas pressure, a quantity equivalent to the (Shakura & Sunyaev 1973) α parameter.

Even with a system as simple as the shearing box, there are many possible factors, both computational as well as physical, that could in principle govern the saturation amplitude. These include the initial field strength and geometry, box size and aspect ratio, value of Ω , background gas pressure, and numerical resolution. Many of these are physically significant only in relation to others. For example, Ω is an arbitrary time scale in the system. The shearing box system is independent of Ω so long as q remains constant and the physical box size changes proportionately. The formal scaling invariance is that if

$$\Omega \rightarrow c\Omega, \quad (11)$$

where c is an arbitrary constant, then the equations remain unchanged if

$$(x, t) \rightarrow (x/c, t/c). \quad (12)$$

We will make use of this fundamental property in §4 when we explore chaotic behavior.

For the cases of an initial uniform field oriented along either the y or z axes, Hawley, Gammie & Balbus (1995) found that the saturation amplitude of the turbulence depended upon both the box size and initial field strength. When the field had a vanishing mean value over the computational box volume, the final outcome was much less sensitive to the initial field energy. Here, we present a series of zero mean field simulations designed to test how the box size affects the overall level of the turbulence. The baseline calculation has $q = 1.5$ corresponding to a Keplerian background, and a box size of $L_x = 1$, $L_y = 2\pi$, and $L_z = 1$, set so that $L_z = c_s^2/\Omega$ where $c_s^2 = P/\rho$. The actual values used are $P = 10^{-6}$ and $\Omega = 0.001$. The gas is adiabatic with $\gamma = 5/3$. The initial field is vertical and varies sinusoidally in the x direction, $B_z \propto \sin(x/L_x)$. The field strength set so that the volume average magnetic energy corresponds to $\beta = 800$. The maximum vertical field has $\beta = 400$, which gives a fastest growing wavelength for the MRI of $\lambda_{\max} = 8\pi/15^{1/2}(v_A/\Omega) = 0.46$. The grid resolution is $32 \times 64 \times 32$ zones in (x, y, z) . This setup corresponds to the so-called “fiducial box” used in Hawley, Gammie & Balbus (1995, 1996) and Brandenburg et al. (1995).

In addition to the fiducial run, we computed four additional simulations with different box dimensions. In three simulations we doubled each of the box dimensions in turn, and in the final simulation of this set we quadrupled the vertical size. To maintain a constant resolution number of grid

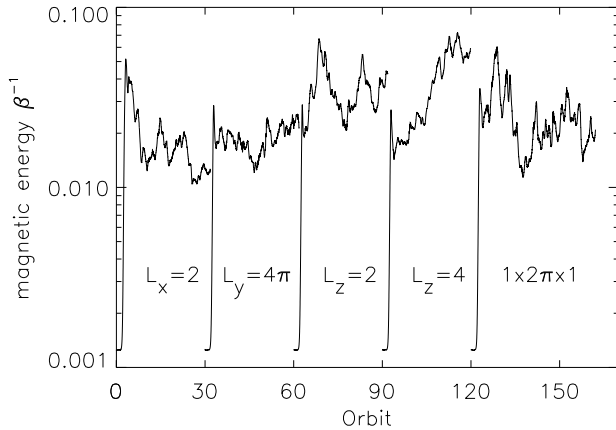


Figure 1. Magnetic energy histories for an ensemble of shearing box runs with different box sizes. Magnetic energy is expressed in terms of the ratio of the magnetic pressure to initial gas pressure, β^{-1} . The zero point in time for each run is offset by 30 orbits for ease of comparison. Each curve is labeled by the dimension that is increased. The fiducial box is the rightmost plot.

zones per unit length, the number of grid zones used was increased appropriately. Figure 1 shows the magnetic energy per unit volume evolving over 30 orbits for each run in this series of models. While one must be cautious extrapolating from this limited time baseline, the results generally suggest that increasing the vertical dimension is the most important effect over the long term. The temporal variations in magnetic energy within a given run are, however, quite large, often well in excess of the running average.

To isolate the effect of the vertical size, we carried out a second set of simulations in which L_z is varied, from $L_z = 1/4$ to $L_z = 4$, and all other factors are held fixed, including the grid zone size Δz . The initial magnetic field is as described above. Here we used an isothermal equation of state, $\gamma = 1.0$ which keeps the box from heating due to dissipation of the turbulence. Figure 2 shows the time evolution of the magnetic energy and even over a limited time baseline clearly reveals a general trend toward increasing magnetic energy with increasing z box size, again with significant variation. The most striking conclusion is that there is a lower bound to the vertical size required for amplification to occur: the field energy declines dramatically in the $L_z = 1/4$ model, and even the initial linear growth rate is reduced. The fastest growing vertical wavelengths for initial field strengths with $\beta < 1350$ no longer fit inside the box, and evidently losses win over the reduced power input at the top of the turbulent cascade.

For box sizes $L_z = 1/2$ and larger the turbulence is sustained over the evolution period of 30 orbits. However, other trends are visible. First, the amplitude of the initial spike of linear growth saturation decreases with increasing L_z . Second, the amplitude of the magnetic energy variations in the turbulent state is reduced with increasing box size.

These history plots demonstrate that it is not a simple matter to quantify the saturation amplitude of the turbulence in a shearing box, or to determine unambiguously the influence of physical parameters in setting that ampli-

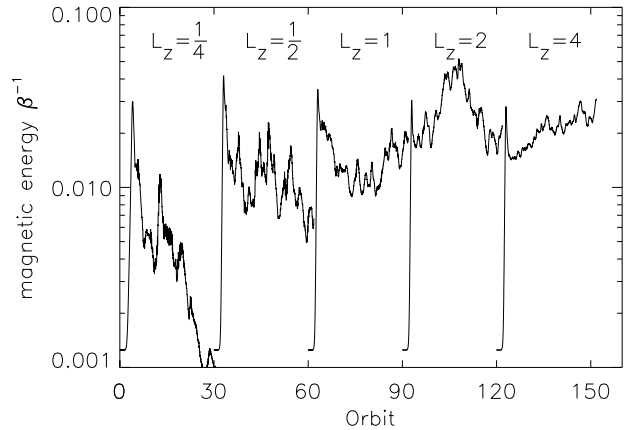


Figure 2. Magnetic energy histories for an ensemble of shearing box runs with different vertical box sizes. Magnetic energy is expressed in terms of the ratio of the magnetic pressure to initial gas pressure, β^{-1} . The zero point in time for each run is offset by 30 orbits for ease of comparison. Each curve is labeled by the value of L_z .

tude. It is not obvious, in general, over what length of time one should average to obtain a characteristic amplitude; nor is it even obvious that such a baseline must always exist. Large fluctuations, even in volume-averaged data, are the rule. This is the overarching and defining characteristic of the MHD turbulence: it is chaotic.

4 ONSET OF CHAOS

It is clear that changing the physical parameters of a shearing box run can result in different levels of turbulence. Here we show that almost exactly the *same* physical parameters, but with tiny variations in numerical value, leads to macroscopically different levels of turbulence. The sensitivity of the system to infinitesimal perturbations is a key feature of chaos.

The first set of simulations consists of three shearing boxes with different Ω values, but which have been rescaled so as to be physically equivalent. All three have $q = 1.5$, $\beta = 800$, $\gamma = 1.0$, $B_z \propto \sin(x/L_x)$, and $32 \times 64 \times 32$ grid zones. One run uses the standard box size of $1 \times 2\pi \times 1$ with $\Omega = 0.001$. The other two have $\Omega = 0.0031$ and $\Omega = 0.000507$ with the physical box sizes scaled accordingly.¹ An identical sinusoidal velocity perturbation was applied to the initial state in each box. In principle, since the length to time ratio is preserved between these different shearing box systems, the resulting evolution should be identical. In the computational experiment, however, these scaled systems evolved very differently.

Figure 3 shows the volume averaged magnetic energy density histories for the three runs. The initial linear growth

¹ Care must be taken so that the rescaling does not correspond to a simple shift by an integer number of bits in the machine registers.

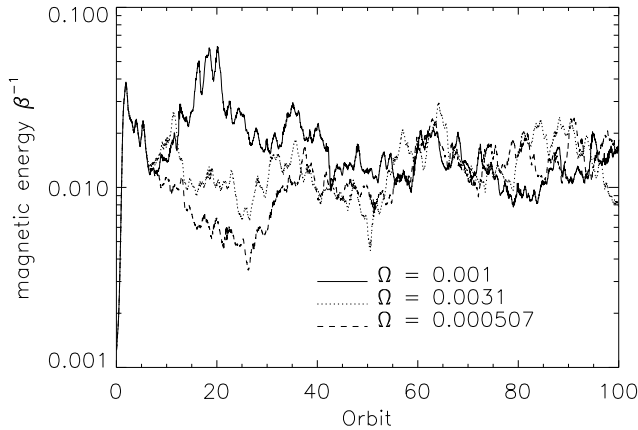


Figure 3. Time evolution of the magnetic energy for a series of simulations with different Ω values, with the box dimensions adjusted so that each run is formally equivalent. Despite this, the magnetic energies diverge after the initial linear growth and saturation.

and saturation phase is indistinguishable. Significant deviations appear after orbit 8, and at orbit 20 the energies are widely different. Since these simulations correspond to identical physical conditions, one might expect that, at the very least, time-averaged values would coincide. Figure 4 illustrates how the running time averages of the volume-averaged stress parameter α for each run evolves with time. The running time average is defined

$$\langle \alpha(t) \rangle = \frac{1}{(t - t_o)} \int_{t_o}^t \alpha dt, \quad (13)$$

and the expectation is that this should converge to a steady value characteristic of the turbulence. The question is, over what time interval should this happen? As figure 4 shows, the fluctuations in the stress are so large that the running time averages $\langle \alpha(t) \rangle$ do *not* coincide. Since a very large excursion in magnetic energy is visible in figure 3 at 20 orbits, we computed the running average from 45 to 120 orbits. But over this interval a unique characteristic α does not emerge even for a single simulation.

The next experiment further demonstrates the chaotic nature of the turbulence by taking the data halfway through an extended run and randomly perturbing the flow velocities with a gaussian rms value of 0.001%. The subsequent evolution is then compared with the extended run. The parameters for this test were $\Omega = 0.0005$, $q = 1.5$, $\beta = 400$, $\gamma = 1.0$, $B_z \propto \sin(x/L_x)$, grid size of $32 \times 64 \times 32$, and an appropriately scaled box equivalent to the standard box. The results are shown in figure 5. The arrow indicates the time when the perturbations were added, and the perturbed simulation was then run on to 60 orbits in time. The plot of magnetic energy reveals a visible divergence by orbit 30, and a substantial difference by orbit 35. This is the defining feature of chaos: substantially different macroscopic behavior created by infinitesimal perturbations.

To compare the behavior of models with different initial field topologies, we perform an experiment with an initial uniform toroidal magnetic field for two boxes, one with

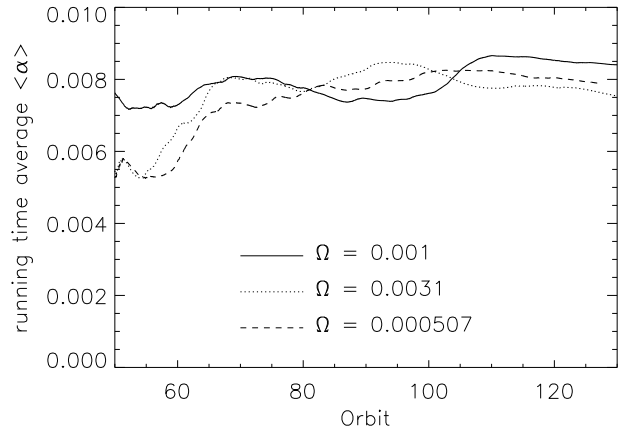


Figure 4. Running time averages of α for the three simulations with different Ω values. The averages are computed beginning with orbit 45, well after turbulence is established. This shows that the average α values only slowly converge to comparable time-averages even after 120 orbits.

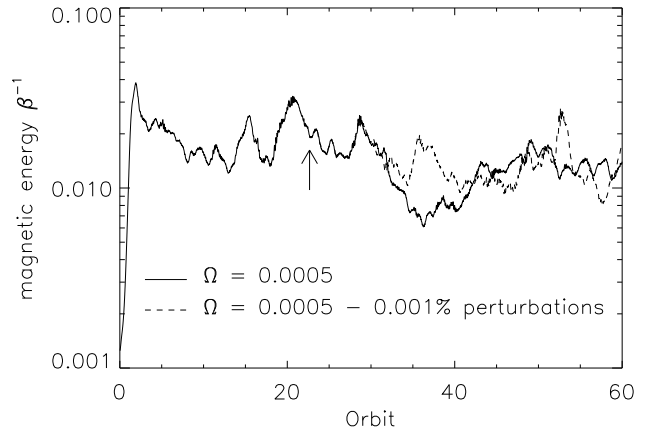


Figure 5. The evolution of a baseline simulation (solid line) and a comparison simulation to which small velocity perturbations are added (dashed line). Data from the baseline simulation are perturbed at the 0.001% level at the point in time indicated by the arrow. The resulting magnetic energy histories diverge visibly by 30 orbits, and are markedly different by 35 orbits.

$\Omega = 0.001$ the other with $\Omega = 0.0031$. Other physical parameters were the same as in the vertical field experiments. Figure 6 displays the volume-averaged magnetic energy density histories for these runs. Again, the initial linear growth phases of the two runs were identical; diverging behavior is a nonlinear phenomenon. The amplitude of the variations is not as great as in the vertical field case. Nevertheless, as figure 7 shows, the running time averages of α required 100 orbits to converge.

As a contrast to the chaotic behavior of MHD turbulence, we also ran several purely hydrodynamic shearing box systems. Hydrodynamic shearing boxes are linearly stable when $q < 2$ (the Rayleigh criterion), and nonlinearly stable when $q < 2 - \epsilon$, where ϵ is a number on order 0.01

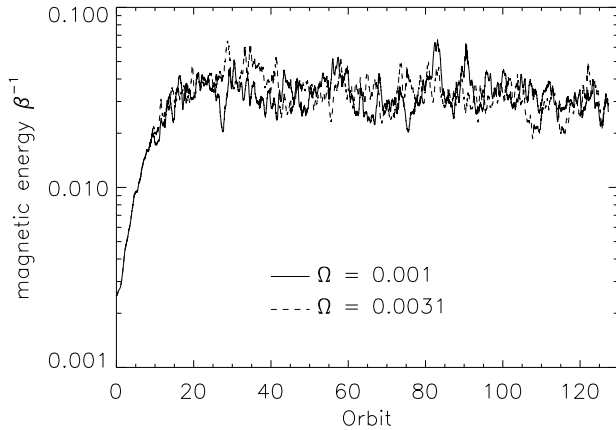


Figure 6. Volume averaged magnetic energy as a function of time for two different Ω simulations with an initial uniform toroidal (y) magnetic field. Magnetic energy is expressed in terms of the ratio of the magnetic pressure to initial gas pressure, β^{-1} .

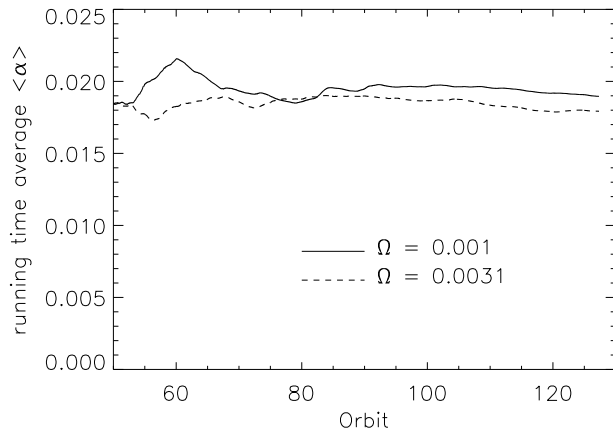


Figure 7. Running time averages of α for two toroidal field simulations with different Ω values. The averages are computed beginning with orbit 45, well after turbulence is established. The time averages approach different values by 120 orbits.

(Hawley, Balbus, & Winters 1999). All of the $q = 1.5$ hydrodynamical simulations gave similar results. The volume-averaged kinetic energies die out in an identical fashion for equivalent problems that use different Ω values. Small fluctuations exist in the form of waves, and are typical of decaying hydrodynamic turbulence. These waves were reproduced almost identically from simulation to simulation—the measured differences were consistent with round-off error. Additional experiments with different q parameters (up to $q = 1.95$) were carried out, and all of these stable hydrodynamical experiments remained identical in their macroscopic properties. The numerical differences were small, not increasing, and consistent with machine precision. These results are consistent with the conclusion that the observed chaos is indeed a property of the MHD turbulence, not of the shearing box itself or the numerics.

4.1 Lyapunov Exponents

The experiments provide compelling, but qualitative evidence that MRI-driven MHD turbulence is chaotic. A more quantitative parameterization of chaotic behavior is afforded by the use of Lyapunov exponents. A system with N degrees of freedom has N Lyapunov exponents. The largest positive exponent represents the average rate of divergence of two initially close evolution paths in phase space. The evolution paths are traced out by monitoring the state vector of the system, which we define as

$$\mathbf{v} = \left(v_x, v_y, v_z, \frac{B_x}{\sqrt{4\pi\rho}}, \frac{B_y}{\sqrt{4\pi\rho}}, \frac{B_z}{\sqrt{4\pi\rho}} \right). \quad (14)$$

The density itself is generally of secondary importance, and therefore is tracked only indirectly in the Alfvén velocity. Close evolution paths imply that there are small differences between the state vectors for each of the two trajectories. If an initially small difference diverges exponentially between two state vectors, the system is formally chaotic. This corresponds to a positive Lyapunov exponent.

Kurths & Brandenburg (1991) demonstrated chaos in MHD solar convection simulations in three-dimensions and computed estimates of the Lyapunov exponents. We follow their procedure to perform a similar analysis for MRI-driven turbulence. We begin with an evolution in which MHD turbulence has fully developed. Then, a second evolution path is created by randomly perturbing the velocity components of the first system’s state vector. The two state vector trajectories are then evolved for about 4 orbits, and, at regular time intervals the fractional state vector difference between the two paths was calculated:

$$\delta = \frac{|\mathbf{V}_p - \mathbf{V}|}{|\mathbf{V}|} \quad (15)$$

where \mathbf{V}_p and \mathbf{V} are the perturbed and original state vectors. Data from the last two orbits in the state vector difference history are then fit to an exponential from which we estimate the value of the largest Lyapunov exponent.

In the first experiment we employ a standard shearing box, namely $1 \times 2\pi \times 1$, grid size of $32 \times 64 \times 32$, with an isothermal equation of state, $\gamma = 1.0$, sinusoidal vertical field, $B_z \propto \sin(x/L_x)$, of average magnetic energy $\beta = 800$, and a background Keplerian shear, $q = 1.5$. This was evolved until MHD turbulence had fully developed. Perturbations were then applied to a parallel computation and the state vector difference was calculated as a function of time. The resulting Lyapunov exponent is $0.458\omega_{\max}$, where $\omega_{\max} = 0.75\Omega$ is the maximum unstable growth rate for the *linear phase* of magnetorotational instability (Balbus & Hawley 1998). All of our experiments yield a Lyapunov exponent comparable to ω_{\max} .

That the Lyapunov exponent would be on order of the maximum MRI growth rate is not surprising. It is precisely the linearly unstable, exponentially growing MRI that is feeding the turbulence, and driving exponential divergence of the state vector. To examine this more carefully, a series of experiments was performed on shearing boxes with a variety of background shear q parameters and for both sinusoidal vertical and toroidal initial field configurations. Because the maximum linear growth rate of the MRI is $q/2$ (Balbus & Hawley 1998), the ensemble of simulations spans

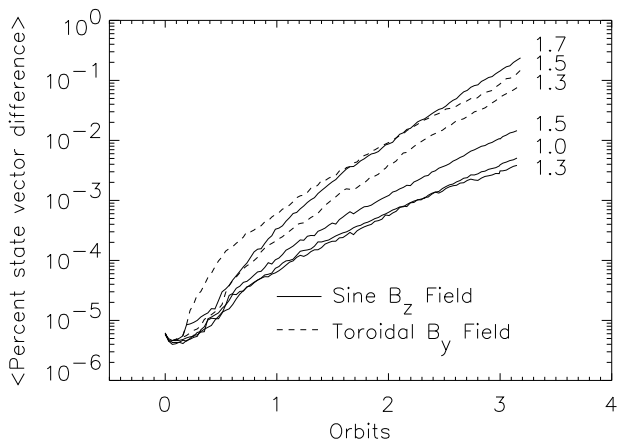


Figure 8. The percent state vector difference histories for a series of vertical field simulations (solid lines) and toroidal field simulations (dashed lines). Each curve is labeled by the background shear parameter q . The exponential divergence that sets the first Lyapunov exponent is clearly seen. The rough trend of larger Lyapunov exponent with increased q value is also visible.

an interesting range of MRI growth rates. We would expect the Lyapunov exponent to be proportional to q as well. Figure 8 displays the volume averaged, percent state vector difference histories for these runs. The curves are labeled by their q values, with solid lines for the vertical field runs and dashed lines for the toroidal field runs. The corresponding first Lyapunov exponent values normalized by ω_{\max} are 0.521, 0.458, 0.422 and 0.583 for the vertical field cases, in order of descending q value, and 0.484 and 0.644 for the toroidal field $q = 1.5$ and $q = 1.3$ runs. Clearly, the first Lyapunov exponents are positive, and of the same magnitude, normalized by ω_{\max} . It should also be noted that first Lyapunov exponents were calculated at many points in time in the simulations, always with similar results.

In summary, the Lyapunov exponents in MRI-driven MHD turbulence simulations are all positive, and, when normalized by ω_{\max} , they all lie within a range of 0.4 to 0.6. There is a slight trend of larger Lyapunov exponent for larger q value (non-normalized). Previous experiments also found stronger overall levels of turbulence with larger q values (Hawley, Balbus, & Winters 1999); in a sense, a larger Lyapunov exponent is “more turbulent.” Finally, the chaos parameters of the turbulence are independent of the initial magnetic field configuration. Initial vertical magnetic fields have similar Lyapunov exponent values as initial toroidal magnetic fields.

5 CONCLUSIONS

Shearing box simulations of the MRI constitute an excellent numerical laboratory in which to study chaos in turbulent flow. Their compactness and simple boundary conditions make them a very convenient system to study, but they also require care to interpret. For example, the variance of the the flow fluctuations, which may be of direct astrophysical interest because of its connection with radiative emission, is a function of the box size adopted (cf. figure 2).

In this paper, we have demonstrated the extreme sensitivity of MHD turbulence to infinitesimal deviations in the flow. This was done by several different methods: showing that invariant scaling laws fail when implemented numerically, for both vertical and toroidal initial fields, and externally imposing tiny perturbations on an established turbulent flow and following the growing deviations in the subsequent evolution of the original and the perturbed system. Estimates of the largest Lyapunov exponent in a variety of turbulent flows with different field geometries yielded values near the characteristic growth rate of the linear MRI. This is an indication that the linear physics of the instability plays an active role in defining the highly nonlinear turbulent dynamics of these flows. One way this could come about would be if the energy input into a Kolmogorov-like cascade was essentially the linear MRI.

The most important practical consequence of this behavior is that the nongaussian statistical properties of chaotic flows severely limit the extent to which α modeling can be used uncritically. Though Maxwell and viscous stress have some formal properties in common (Balbus & Papaloizou 1999), the averaging procedure necessary for a semi-local treatment of the turbulence is a very delicate matter. A time base of hundreds of orbits is clearly necessary to establish a meaningful estimate of the characteristic stress. In astrophysical systems, especially those in transience, it may not be possible to ascribe an instantaneous α value to the stress, and there may be no recourse other than detailed numerical modeling.

ACKNOWLEDGEMENTS

We acknowledge support under NSF grant AST-0070979, and NASA grant NAG5-9266. Some of the simulations described here were carried out on computational platforms at the NSF-supported National Center for Supercomputing Applications and the San Diego Supercomputer Center.

REFERENCES

- Balbus, S. A., & Hawley, J. F. 1991, *ApJ*, 376, 214
- Balbus, S. A., & Hawley, J. F. 1998, *Rev. Mod. Phys.*, 70, 1
- Balbus, S. A., & Papaloizou, J. C. B. 1999, *ApJ*, 521, 650
- Brandenburg, A., Nordlund, Å., Stein, R. F., & Torkelsson 1995, *ApJ*, 446, 741
- Hawley, J. F., Balbus, S. A., & Winters, W. F. 1999, *ApJ*, 518, 394
- Hawley, J. F., Gammie, C. F., & Balbus, S. A. 1995, *ApJ*, 440, 742
- Hawley, J. F., Gammie, C. F., & Balbus, S. A. 1996, *ApJ*, 464, 690
- Hawley, J. F., & Stone, J. M. 1995, *Comp Phys Comm*, 89, 127
- Kurths, J., & Brandenburg, A., 1991, *Phys Rev A*, 44, R3427
- Shakura, N. I., & Sunyaev, R. A. 1973, *A&A*, 24, 337
- Stone, J. M., & Norman, M. L. 1992a, *ApJS*, 80, 753
- Stone, J. M., & Norman, M. L. 1992b, *ApJS*, 80, 791